INTERNATIONAL JOURNAL FOR NUMERICAL METHODS IN FLUIDS
Int. J. Numer. Meth. Fluids **29**: 705–718 (1999)

NUMERICAL SIMULATION OF VISCOUS FLOW: BUCKLING OF PLANAR JETS

MURILO F. TOME[a] AND SEAN McKEE[b,*]

[a] *Instituto Superior Técnico, Departamento de Matemática, Av. Rovisco Pais, 1096 Lisboa Codex, Portugal*
[b] *Department of Mathematics, University of Strathclyde, 26 Richmond Street, Livingstone Tower, Glasgow G1 1XH, UK*

SUMMARY

The phenomenon of viscous fluid buckling has a long and distinguished history, dating back to Taylor (1968). This paper is concerned with demonstrating that a numerical method, GENSMAC, is capable of simulating this physical instability. A table of the parameter values (e.g. the Reynolds number, the Froude number, inlet width, inlet velocity and aspect ratio) is provided giving details of when buckling occurs and when it does not. This allows the deduction of a possible buckling condition in terms of the Reynolds number and the ratio of height of the jet to the inlet width, modifying a previous hypothesis. Visualization of jet buckling is provided. This work has been motivated by the need of industry to understand jet filling of containers; jet buckling can lead to air entrapment and this is undesirable.

KEY WORDS: CFD; free-surface flows; jet buckling

1. INTRODUCTION

In 1744, Euler determined the critical load for elastic buckling of a slender column. He found that buckling occurred when $l^2R > \pi^2B$, where R is the axial compressive stress or load, B is the flexural rigidity and l is the length of the column. A similar buckling phenomenon is also known to exist for fluids and as yet, no similar satisfactory mathematical theory exists to describe the phenomenon. It manifests itself by the coiling or folding of a thin stream onto a flat plate just as honey does 'falling' from a spoon. This paper is concerned with a modest contribution to this problem: a critical stability region specifying when the fluid jet will buckle has been found through extensive numerical experimentation.

Taylor [1] was the first to study this phenomenon. Then followed a number of related papers, e.g. Lienhard [2], Suleiman and Munson [3], before an extensive experimental examination of jet buckling was carried out by Cruickshank [4]—see also Cruickshank and Munson [5]. Approximate mathematical models have been developed by Cruickshank [6] and Tchavdarov *et al.* [7] and have been shown not to compare too badly with experiments. An exhaustive bibliography can be found in the review article by Bejan [8].

The viscous jet may be either in tension or compression, depending on the velocity gradient along its axis (Cruickshank and Munson [5]). If the diameter of the jet increases in the

* Correspondence to: Department of Mathematics, University of Strathclyde, 26 Richmond Street, Livingstone Tower, Glasgow G1 1XH, UK.

CCC 0271–2091/99/060705–14$17.50
Received July 1995
Revised October 1997

downstream direction, the viscous normal stress along its axis is one of compression. If this viscous compressive component of the normal stress is large enough, the net axial stress in the jet may be compressive. Thus, near the flat plate, sufficiently large axial compressive stresses, along with a sufficiently 'slender' jet, combine under appropriate circumstances to produce the fluid mechanics analog to the elastic buckling of a slender solid column.

The motivation for this work came from the authors' involvement with a large food processing company. One of the problems associated with the jet filling of containers is air entrapment and this may occur during jet buckling. Thus, the purpose of this paper is first to demonstrate that, by solving the two-dimensional time-dependent Navier–Stokes equations, this buckling phenomenon—a non-linear physical instability—can be simulated; and secondly, to provide a table of parameter values of the system for when buckling occurs and when it does not. This table then allows the deduction of a relationship between the Reynolds number and the ratio of the height of the jet and the inlet width for which buckling will or will not occur. This modifies a hypothesis of Cruickshank [6], which he arrived at through experimentation and a one-dimensional stability analysis. An extensive experimental program has already been carried out to validate the code and this is reported in Barrat *et al.* [13].

This paper only describes the essential steps of the numerical method; details of the methodology employed can be found in Tome [9] and Tome and McKee [10].

2. BRIEF DESCRIPTION OF THE GENSMAC CODE

The GENSMAC code solves the two-dimensional time-dependent Navier–Stokes equations for an incompressible viscous fluid. It is an updated version of the SMAC (simplified marker and cell) method (Amsden and Harlow [11]) for calculating time-dependent free-surface flow problems employing pressure and velocity as the primary dependent variables. It employs a finite difference approach on a staggered grid. An adaptive time stepping technique (see [10]) has been used and a conjugate gradient solver is employed to invert the discrete Poisson equation. The code is designed to deal with free-surface flows within a general domain with free-slip or no-slip rigid boundaries. A number of inflows and outflows can be handled, as can any number of internal obstacles.

2.1. Basic equations

The basic equations are the two-dimensional time-dependent Navier–Stokes equations together with the mass conservation equation, which in non-dimensional form can be written as:

$$\frac{\partial u}{\partial t}+\frac{\partial u^2}{\partial x}+\frac{\partial uv}{\partial y}=-\frac{\partial p}{\partial x}+\left(\frac{1}{Re}\right)\frac{\partial}{\partial y}\left(\frac{\partial u}{\partial y}-\frac{\partial v}{\partial x}\right)+\frac{1}{Fr^2}g_x, \tag{1}$$

$$\frac{\partial v}{\partial t}+\frac{\partial uv}{\partial x}+\frac{\partial v^2}{\partial y}=-\frac{\partial p}{\partial y}-\left(\frac{1}{Re}\right)\frac{\partial}{\partial x}\left(\frac{\partial u}{\partial y}-\frac{\partial v}{\partial x}\right)+\frac{1}{Fr^2}g_y, \tag{2}$$

$$\frac{\partial u}{\partial x}+\frac{\partial v}{\partial y}=0, \tag{3}$$

where $Re = UL/v$ and $Fr = U/\sqrt{Lg}$ are the associated Reynolds number and Froude number respectively. U and L are typical velocity and length scales and v is the kinematic viscosity, g is the gravitational constant with $\mathbf{g} = (g_x, g_y)^T$ the unit gravitational field vector, $\mathbf{u} = (u, v)^T$ are the non-dimensional components of velocity, while p is the non-dimensional pressure per unit density.

2.2. Solution procedure

The solution procedure is based on the sequential solution at each time step of an explicit discretization of the Navier–Stokes equations followed by a discretized Poisson equation for a corrected velocity potential, ψ. Solving the Navier–Stokes equations for $\tilde{\mathbf{u}}(\mathbf{x}, t)$, say with the correct boundary conditions, creates the correct vorticity, but mass is not conserved. This is achieved by writing

$$\mathbf{u}(\mathbf{x}, t) = \tilde{\mathbf{u}}(\mathbf{x}, t) - \nabla\psi,$$

so that $\nabla\cdot\mathbf{u}(\mathbf{x}, t) = 0$ whenever

$$\nabla^2\psi = \nabla\cdot\tilde{\mathbf{u}}(\mathbf{x}, t).$$

It is supposed that at a given time t_0, the velocity field $\mathbf{u}(\mathbf{x}, t_0)$ is known and boundary conditions for velocity and pressure are given. The updated velocity field $\mathbf{u}(\mathbf{x}, t)$ at $t = t_0 + \delta t$ is calculated as follows:

1. Let $\tilde{p}(\mathbf{x}, t_0)$ be a pressure field that satisfies the correct pressure condition on the free surface.
2. Calculate the intermediate velocity field $\tilde{\mathbf{u}}(\mathbf{x}, t)$ from the explicit discretized form of

$$\frac{\partial\tilde{u}}{\partial t} = \left[-\frac{\partial u^2}{\partial x} - \frac{\partial uv}{\partial y} - \frac{\partial\tilde{p}}{\partial x} + \left(\frac{1}{Re}\right)\frac{\partial}{\partial y}\left(\frac{\partial u}{\partial y} - \frac{\partial v}{\partial x}\right) + \frac{1}{Fr^2}g_x \right]_{t=t_0}, \tag{4}$$

$$\frac{\partial\tilde{v}}{\partial t} = \left[-\frac{\partial uv}{\partial x} - \frac{\partial v^2}{\partial y} - \frac{\partial\tilde{p}}{\partial y} - \left(\frac{1}{Re}\right)\frac{\partial}{\partial x}\left(\frac{\partial u}{\partial y} - \frac{\partial v}{\partial x}\right) + \frac{1}{Fr^2}g_y \right]_{t=t_0}, \tag{5}$$

   where $\mathbf{u}(\mathbf{x}, t_0) = (u, v)^T$ using the correct boundary conditions for $\mathbf{u}(\mathbf{x}, t_0)$.
3. Solve the Poisson equation

$$\nabla^2\psi = \nabla\cdot\tilde{\mathbf{u}}(\mathbf{x}, t). \tag{6}$$

4. Compute the velocity

$$\mathbf{u}(\mathbf{x}, t) = \tilde{\mathbf{u}}(\mathbf{x}, t) - \nabla\psi.$$

5. Compute the pressure

$$p = \tilde{p} + \frac{\psi}{\delta t}.$$

As the time integration of the intermediate velocity field is performed by an explicit method, the local truncation error is $O(\delta t)$. It is well-known that for this scheme to be stable, certain time stepping restrictions need to be satisfied [10]. This can lead to small time steps (of the order of 10^{-5}), although these are to some extent mitigated by the automatic time stepping routine. In designing this code, the authors primarily sought robustness with respect to a wide range of Reynolds numbers; in addition, to maintain accuracy, the mesh spacings chosen were often small (a grid of 100×100 was employed throughout this paper). Consequently, computing times can be large with some of the runs taking 20 h on a Dec alpha 600.

2.3. Boundary conditions

There are several types of conditions that can be applied at the boundary, namely: no-slip, free-slip, prescribed inflow, prescribed and continuative outflow. For a detailed discussion see [9]. The appropriate boundary condition for the Poisson equation (Amsden and Harlow [11]) is

$$\frac{\partial \psi}{\partial n} = 0,$$

on the mesh boundary and $\psi = 0$ on the free-surface. The free-surface boundary conditions are the vanishing of the normal and tangential stresses, which can be expressed as [12]:

$$p - (2/Re)\left[n_x^2 \frac{\partial u}{\partial x} + n_x n_y \left(\frac{\partial u}{\partial y} + \frac{\partial v}{\partial x} \right) + n_y^2 \frac{\partial v}{\partial y} \right] = 0, \tag{7}$$

$$(1/Re)\left[2 n_x m_x \frac{\partial u}{\partial x} + (n_x m_y + n_y m_x) \left(\frac{\partial u}{\partial y} + \frac{\partial v}{\partial x} \right) + 2 n_y m_y \frac{\partial v}{\partial y} \right] = 0 \tag{8}$$

respectively, where n and m are the normal and tangential direction cosines to the surface respectively. These conditions are applied by making local finite difference approximations on the free-surface [10].

2.4. Marker particles

Marker particles are used to represent the fluid itself. Their essential task is to provide the position of the moving free-surface so that the stress conditions can be applied accurately. They are updated at the end of each calculational time step so as to provide the dynamics of the fluid motion.

The new particle co-ordinates are found by solving

$$\frac{\mathrm{d}x}{\mathrm{d}t} = u \quad \text{and} \quad \frac{\mathrm{d}y}{\mathrm{d}t} = v$$

using Euler's method. Thus, after the velocity field is updated, the particles are moved according to

$$x_p^{n+1} = x_p^n + u_p \delta t^{n+1},$$
$$y_p^{n+1} = y_p^n + v_p \delta t^{n+1},$$

where (x_p^n, y_p^n) is the current particle position, δt^{n+1} is the actual time step employed and (x_p^{n+1}, y_p^{n+1}) is the particle's updated position.

The velocities u_p and v_p are found from a bilinear approximation using the four nearest u and v velocities.

3. JET BUCKLING: A NUMERICAL EXPERIMENT

The experimental results of Cruickshank and Munson [5] suggest that buckling will occur when the Reynolds number (Re) averages about 0.56 or less. A pertubation analysis of Cruickshank [6] suggests that the condition for buckling is given by

$$H/D = (2n + 1)\pi \quad (n = 0, 1, \ldots),$$

where D and H are the slit width and the height of the inlet to the plate respectively. Experimental evidence, provided by Cruickshank and Munson [5], then leads Cruickshank [6] to suggest that buckling of a planar jet appears to occur when $n = 1$, i.e. when H/D is greater than 3π. Thus, from their experimental results, they deduced that buckling will probably occur when the Reynolds number is less than 0.56 and the ratio H/D is greater than 10.

Based on these assumptions, a series of runs were performed using the GENSMAC code in order to make a comparison with experimental results. The following numerical experiment was carried out.

An empty rectangular cavity with the no-slip condition imposed on its walls is considered. Through an inlet, a thin jet of fluid is injected into the cavity at a constant velocity. The cavity is chosen to be sufficiently wide to permit buckling without the jet touching the cavity walls. The geometry of the experiment is shown in Figure 1, where again D is the inlet size and H is the height of inlet jet from the bottom wall of the cavity. The values of H, inlet size D, inlet velocity U and the kinematic viscosity v, assume several values within the runs. The following data were employed:

$$D = 3, 4, 5 \text{ mm}, \quad U = 0.5, 1.0 \text{ m s}^{-1}, \quad v = 0.005, 0.010, 0.020 \text{ m}^2 \text{ s}^{-1}.$$

These gave Reynolds numbers Re, based on the slit width, in the range of [0.075, 1.0] and Froude numbers Fr in the range [2.258, 5.829]. The height H was in the range [3.0, 24.0] cm, in which case the ratio H/D took values in the range [9.0, 80.0]. A selection of the results is displayed in Table I. Figure 2 displays a particular buckling obtained for the data $H/D = 12.5$, $D = 4$ mm, $U = 0.5$ m s^{-1} and $v = 0.010$ m^2 s^{-1} ($Re = 0.20$, $Fr = 2.524$). Results for a jet that shows no signs of buckling are displayed in Figure 3, for the data $H/D = 11.0$, $D = 4$ mm, $U = 0.5$ m s^{-1} and $v = 0.005$ m^2 s^{-1} ($Re = 0.4$, $Fr = 2.524$).

Table I sets out the results of a selected number of the simulations performed. It is clear that the Reynolds number is an important factor in the buckling phenomenon. Note that for $Re > 0.60$ (more detailed runs, not displayed here, suggest $Re > 0.56$) buckling does not occur. However, for aspect rations of around 10 and $Re = 0.50$, buckling also does not occur, but does occur as the aspect ratio is increased, suggesting that the aspect ratio is also significant. To emphasize this point, runs were performed with the following data: $H/D = 10$, $D = 5$ mm, $U = 1.0$ m s^{-1} $v = 0.010$ m^2 s^{-1}, giving $Re = 0.50$ and $Fr = 4.515$; and $H/D = 10$, $D = 5$ mm, $U = 0.5$ m s^{-1}, $v = 0.010$ m^2 s^{-1} giving $Re = 0.25$ and $Fr = 2.258$. Buckling did not occur in both cases. However, re-runs with H/D equal to 14.0 and 16.0 respectively, did display buckling; the results for the latter are displayed in Figure 4. There are small, but essential differences between the two runs displayed in Figures 2 and 4. Both initially display a small amount of jet thinning, although this is more pronounced in the run shown in Figure 4, possibly due to the smaller Froude number. After the jet has impacted on the surface, Figure 2 more clearly displays jet thickening; this moves back up the jet prior to buckling. This effect was reported by Cruickshank and Munson [5]. Finally, Figure 4 shows the fluid buckling to the right, whereas in Figure 2, the fluid buckles to the left. This confirms the authors intuition: as with the elastic buckling of a slender rod, the fluid has no propensity to buckle in any preferred direction. This, therefore, verifies that the code is working properly, containing no spurious asymmetric features.

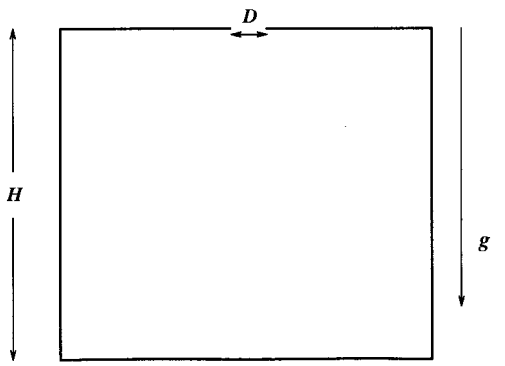

Figure 1. The geometry of the experiment.

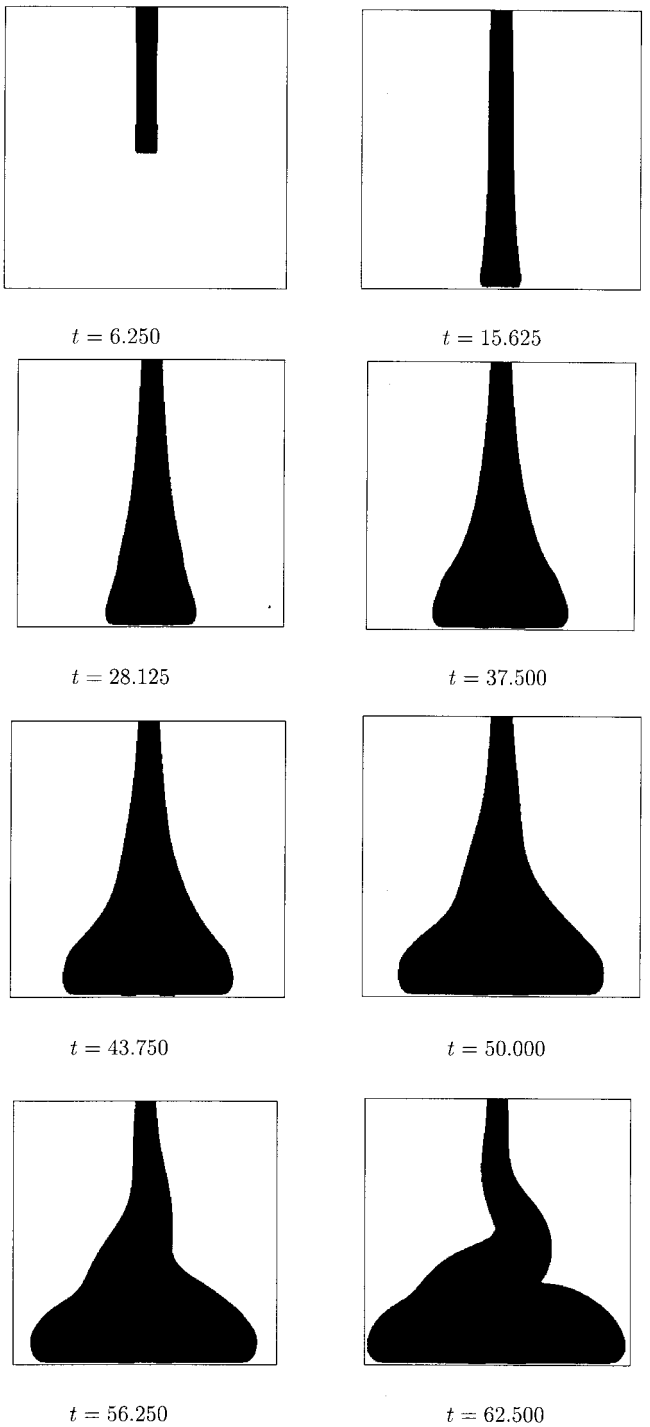

Figure 2. Buckling jet ($Re = 0.20$, $Fr = 2.524$, $H/D = 12.5$); $t = 6.250$, 15.625, 28.125, 37.500, 43.750, 50.000, 56.250, 62.500, 68.750, 75.000, 81.250, 87.500.

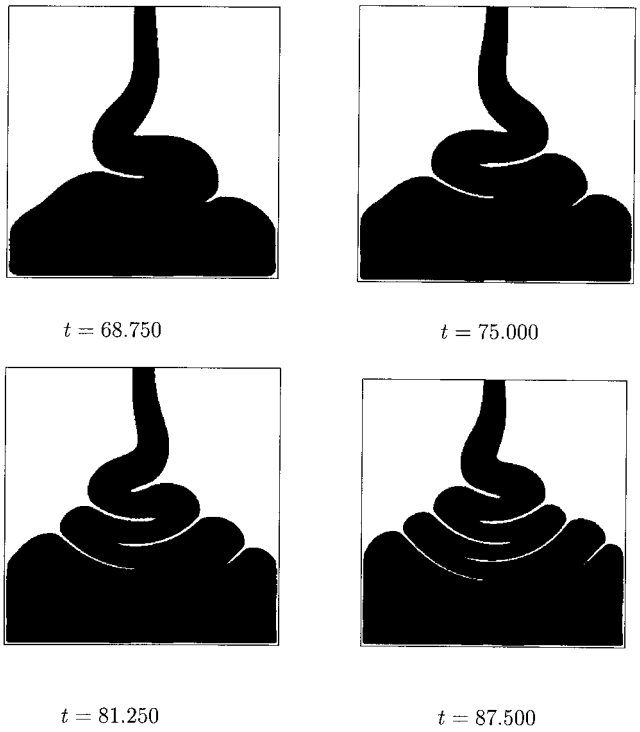

Figure 2 (*Continued*)

Following Cruickshank, it would appear that buckling is primarily dependent on the Reynolds number and the ratio of the height of the jet to the inlet width. A plot, Graph 1, has therefore been made in the (Re, H/D) parameter space of those points which produced buckling (•) and those that did not (●).

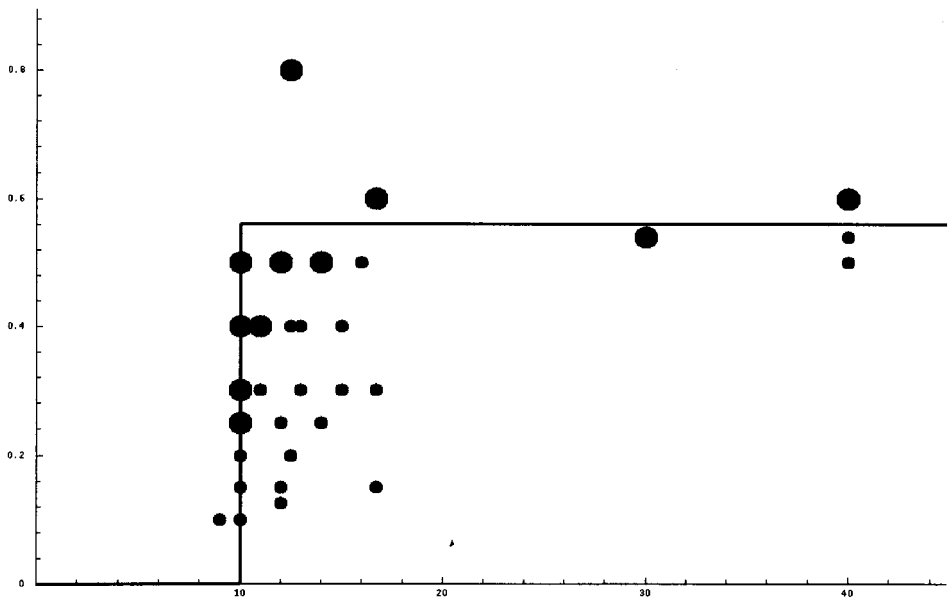

Graph 1. •—Non-buckling points; ●—Buckling points.

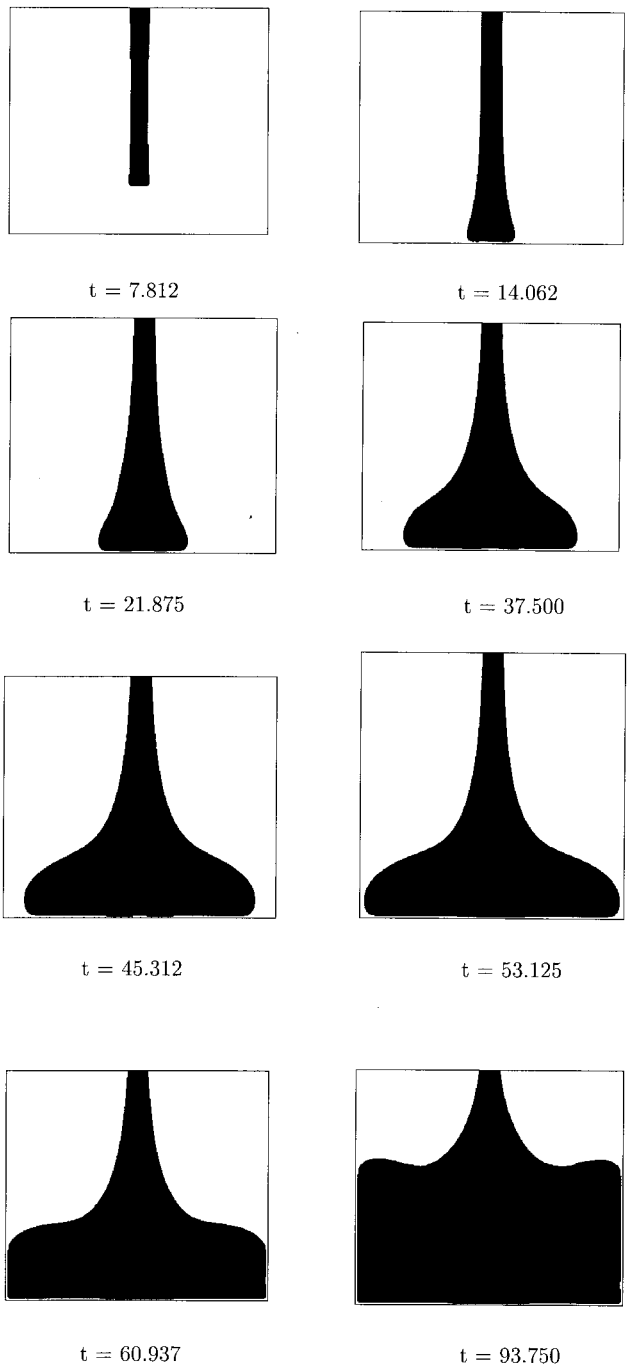

Figure 3. Jet did not buckle ($Re = 0.40$, $Fr = 2.524$, $H/D = 11.0$); $t = 7.812$, 14.062, 21.875, 37.500, 45.312, 53.125, 60.937, 93.750.

Table I

H/D	D (mm)	U (m s^{-1})	v (m^2 s^{-1})	Re	Fr	Result
10.0	3	0.50	0.010	0.15	2.915	B
16.6	3	0.50	0.010	0.15	2.915	B
10.0	3	1.00	0.010	0.30	2.829	nB
11.0	3	1.00	0.010	0.30	5.829	B
13.0	3	1.00	0.010	0.30	5.829	B
15.0	3	1.00	0.010	0.30	5.829	B
16.6	3	0.50	0.005	0.30	2.914	B
16.6	3	1.00	0.010	0.30	5.829	B
16.6	3	1.00	0.005	0.60	5.829	nB
10.0	4	0.50	0.020	0.10	2.524	B
11.0	4	0.50	0.010	0.20	2.524	B
12.5	4	0.50	0.010	0.20	2.524	B
10.0	4	0.50	0.005	0.40	2.524	nB
11.0	4	0.50	0.005	0.40	2.524	nB
12.5	4	0.50	0.005	0.40	2.524	B
13.0	4	0.50	0.005	0.40	2.524	B
15.0	4	0.50	0.005	0.40	2.524	B
12.5	4	1.00	0.005	0.80	5.048	nB
9.0	5	0.50	0.025	0.10	2.258	B
12.0	5	1.00	0.033	0.15	4.515	B
10.0	5	1.00	0.025	0.20	4.515	B
10.0	5	0.50	0.010	0.25	2.258	nB
12.0	5	0.50	0.010	0.25	2.258	B
14.0	5	0.50	0.010	0.25	2.258	B
10.0	5	1.00	0.010	0.50	4.515	nB
12.0	5	0.50	0.005	0.50	2.258	nB
14.0	5	1.00	0.010	0.50	4.515	nB
16.0	5	1.00	0.010	0.50	4.515	B
40.0	5	1.00	0.010	0.50	4.515	B
30.0	5	1.00	0.010	0.54	4.515	nB
40.0	5	1.00	0.009	0.54	4.515	B
40.0	6	1.00	0.010	0.60	4.515	nB

B, jet buckled; nB, jet did not buckle.

Examination of the points in parameter space suggests that there is a critical stability curve separating the two sets. Let the co-ordinates of the buckling points be denoted by $\{x_i, y_i\}$, $i = 1, \ldots, N$, where the aspect ratio H/D is identified as x and the Reynolds number as y. The curve appears to asymptote at $y = 0.56$. Bearing this in mind and the fact that it is parabolic-like, it may be represented by

$$y^2 = \frac{1}{\pi}\frac{(x^c - 8.8^c)}{x^c}, \tag{9}$$

where c is a constant to be determined. This curve will be fitted between the 'buckling' and the 'non-buckling' points. The reason for $1/\sqrt{\pi}$ is the fact that it appears that buckling can only occur if $Re \leq 0.56$; 0.56 is approximately $1/\sqrt{\pi}$. By using the software Mathematica, a value of $c = 2.6$ was found to produce a good fit through the points (see Graph 2). Formula (9) can easily be used by a food processing engineer to avoid jet buckling in his container filling system.

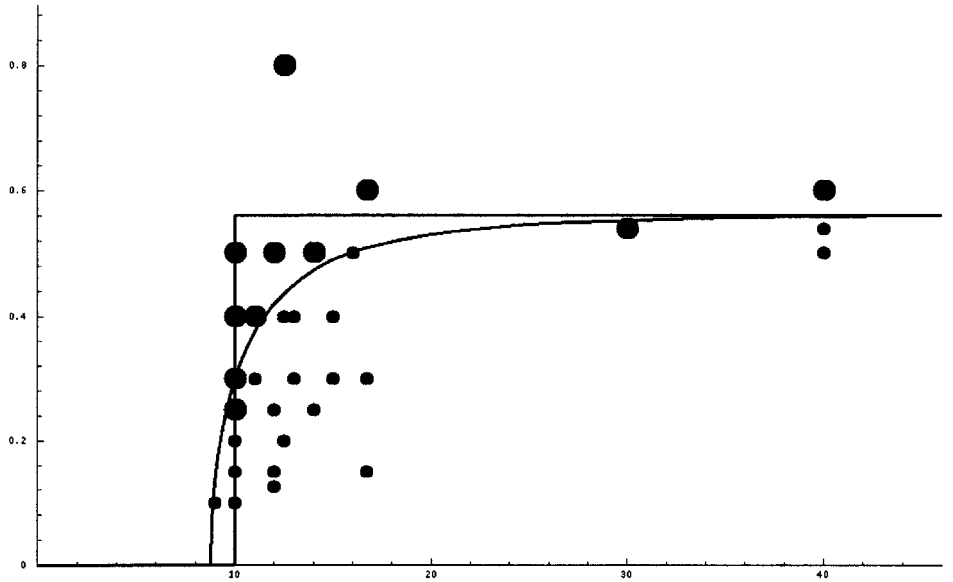

Graph 2. Critical curve defining the buckling region.

3.1. Computational details

Most runs were performed with a $\delta x = \delta y = 1/2$ mm. This gives a mesh size of 100×100 for most runs reported in Table I. The non-dimensional time step size was restricted to

$$\delta t < \frac{1}{8}\frac{\delta x^2}{D} Re,$$

giving a time step size in the range of $[3.130 \times 10^{-4}, 1.250 \times 10^{-3}]$. The average number of cycles for each of the runs was 100000 and the average CPU time taken was 5 h on a Dec Alpha 600. The convergence criteria for the conjugate gradient routine was set to $\epsilon = 10^{-6}$ for all the runs, and the number of iterations taken was usually 2 per cycle; occasionally, the conjugate gradient method took over 10 iterations to satisfy the convergence criteria. Gravity was assumed to act downwards with $g_y = -9.81$ m s^{-2}. The number of particles created at the inlet was four particles for each cell. The visualization was provided by a graphic routine written using the C language and X-windows system.

4. CONCLUDING REMARKS

This paper has been concerned with the use of the code GENSMAC to simulate the viscous buckling of a planar transient jet, and thereby gain further insight into when a fluid jet will buckle. Many runs were performed and a table was constructed displaying a selection of these runs and showing when buckling will occur and when it will not. This in turn has allowed the argument that there is a critical curve in *Reynolds number*/*Aspect ratio* space that defines when buckling might be expected to occur and an approximate curve has been presented. In particular, it was found out that buckling should occur when

$$Re^2 \leq \frac{1}{\pi} \frac{((H/D)^{2.6} - 8.8^{2.6})}{(H/D)^{2.6}}, \tag{10}$$

modifying Cruickshank's hypothesis. Although this represents a best fit of the points displayed in Graph 2, it must be recalled that surface tension has not been included in the numerical simulations, nor indeed has consideration been given to the Froude number (the Froude number is clearly not dominant, but might play a small role in determining whether a jet buckles). Therefore, Equation (10) must be regarded as approximate. Moreover, it is interesting to recall that Euler's stability analysis revealed that a strut would buckle when $l^2R > \pi^2 B$. Since the simulated jet buckling occurs for $H/D > 8.8$ (which, to an engineering approximation, might be taken to be π^2) and $0.56 \approx 1/\sqrt{\pi}$ (see Section 3), the stability condition could be (with a little inspiration from Euler),

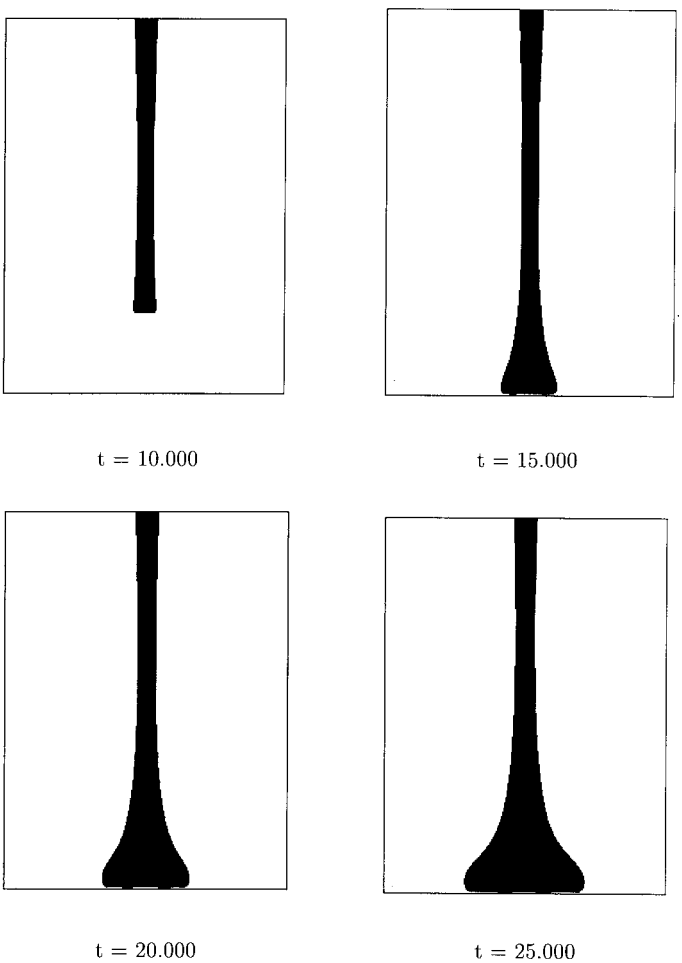

Figure 4. Buckling jet ($Re = 0.5$, $Fr = 2.257$, $H/D = 16.0$); $t = 10.000$, 15.000, 20.000, 25.000, 32.500, 35.000, 40.000, 45.000, 50.000, 60.000, 70.000, 75.000.

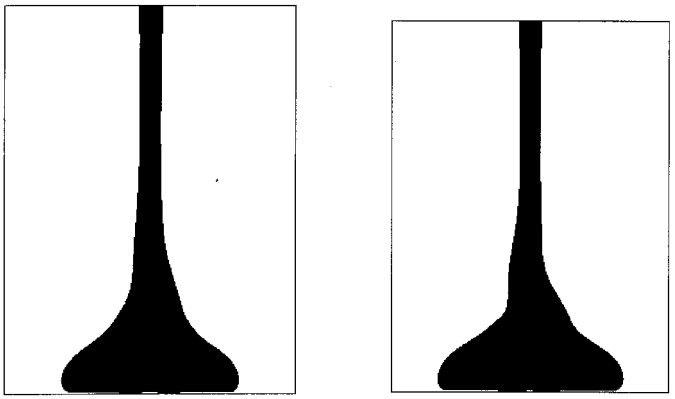

t = 32.500 t = 35.000

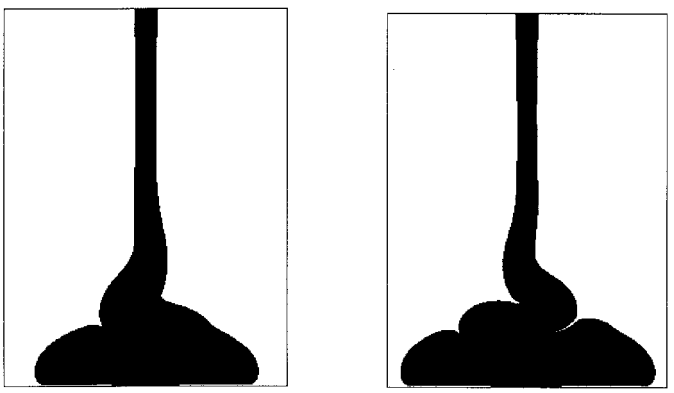

t = 40.000 t = 45.000

Figure 4 (*Continued*)

$$Re^2 \leq \frac{1}{\pi}\left(1 - \frac{\pi^4}{(H/D)^2}\right)$$

or, equivalently,

$$(H/D)^2 \geq \frac{\pi^4}{(1 - \pi Re^2)}.$$

This result provides some, admittedly limited, insight into this problem, but is of real practical value to the food processing engineer concerned with designing a container filling system. However, the reason for studying this problem is arguably more important than this. This problem has so far defied complete mathematical analysis of stability and it is to be hoped that the small contribution given here may act as a guide, or at least a catalyst, to the theoretician. Furthermore, jet buckling is an example of a physical instability; so is turbulence. It is just conceivable that by studying the jet buckling phenomenon and numerical methods that are capable of simulating it, some useful insight may be gleaned about turbulence and how it, and in particular its onset, could be accurately simulated.

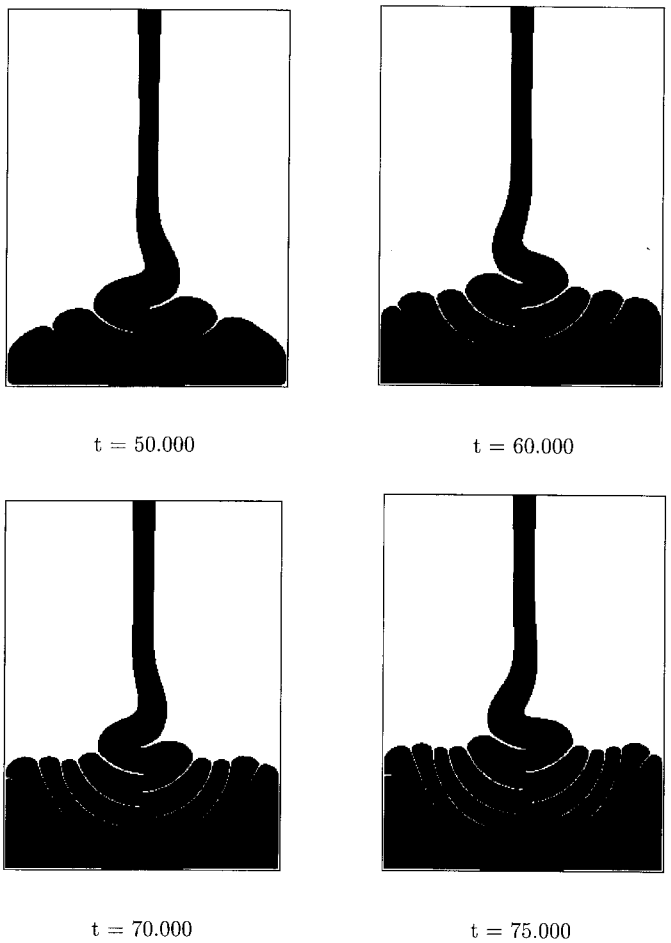

Figure 4 (*Continued*)

ACKNOWLEDGMENTS

The authors wish to thank Dr B. Duffy and Dr S. Wilson, Department of Mathematics, University of Strathclyde, for helpful discussions during the preparation of this work. The authors also wish to thank Dr J. Crilly, Unilever Research for introducing the problem. The first author would like to acknowledge the financial support provided by the Brazilian funding agencies: CNPq—Conselho Nacional de Desenvolvimento Cientifico and FAPESP—Fundação de Amparo a Pesquisa do Estado de São Paulo.

REFERENCES

1. G.I. Taylor, 'Instability of jets, threads and sheets of viscous fluids', *Proc. Int. Cong. Appl. Mech.*, Springer, Berlin, 1968.
2. J.H. Lienhard, 'Capillary action in small jets impinging on liquid surfaces', *J. Basic Eng. Trans. ASME, Series D*, **90**, 137 (1968).
3. S.M. Suleiman and B.R. Munson, *Phys. Fluids*, **24**, 1 (1981).
4. J.O. Cruickshank, *Ph.D. Dissertation*, Iowa State University, Ames, IA, 1980.
5. J.O. Cruickshank and B.R. Munson, *J. Fluid Mech.*, **113**, 221 (1981).
6. J.O. Cruickshank, *J. Fluid. Mech.*, **193**, 111 (1988).

7. B. Tchavdarov, A.L. Yarin and S. Radev, *J. Fluid Mech.*, **253**, 593 (1993).
8. A. Bejan, *Annu. Rev. Numer. Fluid Mech. Heat Transf.*, **1**, 262 (1987).
9. M.F. Tome, *Ph.D. Thesis*, University of Strathclyde, Glasgow, UK, 1993.
10. M.F. Tome and S. McKee, *J. Comp. Phys.*, **110**, 171–186 (1994).
11. A.A. Amsden and F.H. Harlow, 'The SMAC method: a numerical technique for calculating incompressible fluid flows', *Los Alamos Scientific Laboratory Report LA-4370*, Los Alamos, NM, 1970.
12. C.W. Hirt and J.P. Shannon, *J. Comp. Phys.*, **2**, 403 (1968).
13. L. Barrat, D.A. Jarvis, A.J. Patrick, S. McKee and M. Tome, 'An experimental and numerical investigation of container filling', *Int. J. Numer. Methods Fluids* (submitted).

